Received: 19 January 2022 | Revised: 23 May 2022 | Accepted: 18 August 2022

DOI: 10.1002/we.2779

RESEARCH ARTICLE

WILEY

Experimental and numerical investigation of the yaw moment of a downwind coned wind turbine rotor

Christian W. Schulz | Keqi Wang | Klaus Wieczorek | Stefan Netzband | Moustafa Abdel-Maksoud

Institute for Fluid Dynamics and Ship Theory, Hamburg University of Technology, Hamburg, Germany

Correspondence
Christian W. Schulz, Technische Universität Hamburg, 21075 Hamburg, Germany.
Email: christian.schulz@tuhh.de

Funding information
Bundesministerium für Wirtschaft und Energie, Grant/Award Number: 03SX409A-F

Abstract

The yaw moment of wind turbine rotors has never been in the focus of wind turbine aerodynamics. With the increasing activities in the development of support structures for Floating Offshore Wind Turbines (FOWT), which passively align with the wind, the interest has shifted, as an accurate determination of the yaw moment is a crucial issue for a successful design of such power plants. A downwind coned rotor is a promising option to increase the yaw moment and therefore the self-alignment capability of a passively yawing FOWT. Unfortunately, experimental and numerical studies on the estimation of the yaw moment of wind turbine rotors are rare. This is especially the case for downwind coned rotors. The aim of the present work is to provide reliable knowledge in this field. For this purpose, an extensive experimental and numerical study is carried out to determine the yaw moment of a downwind coned rotor. The results obtained from measurements in the wind tunnel are compared to those of simulations using a high fidelity RANS method and a blade element momentum theory (BEMT) method. BEMT is widely applied and can be considered as state of the art for predicting aerodynamic loads on FOWTs. However, the basic assumptions of BEMT do not account for a realistic influence of the skewed wake, so that the application of a correction method is necessary. In this work, the frequently used wake skew correction method based on Pitt and Peters is utilised and its influence on the calculation of the yaw moment is investigated. It is shown that this correction method yields a significant overprediction of the yaw moment in comparison to the measurements and consequently even impairs the quality of the simulation in this case. In contrast to this, the wake-resolving RANS method is capable of reproducing the measurements with reasonable accuracy and provides valuable insight into the role of the lateral force for the measurement of the yaw moment.

KEYWORDS
downwind cone, free yawing, self-aligning wind turbine, wind tunnel, wind turbine aerodynamics, yaw moment

1 | INTRODUCTION

The yaw moment of wind turbine rotors is of special interest for FOWT design and analysis. Most conventional FOWT concepts are equipped with a mooring system that allows small motion amplitudes around the yaw axis during operation. Due to their small hydrodynamic resistance to yaw motion, Spar concepts such as the Hywind Spar[*] in particular are prone to such undesired yaw motion. This problem gains even more importance in the context of wake steering, during which a certain yaw misalignment should be forced to influence the downstream propagation of the wake. To understand and mitigate such motion, it is crucial to determine the rotor yaw moment as it is one of the key influence factors for this phenomenon. Besides the general importance of the rotor yaw moment for FOWT motions, the motion behaviour of passively yawing FOWTs, a comparably new and promising type of FOWT, is affected even more strongly by this moment. Current concepts (eg. SCD nezzy[†], SWAY[‡], X1Wind[§], EOLINK[¶] and SelfAligner by CRUSE Offshore[#]) abandon the yaw bearing while the complete platform can rotate around a single mooring point instead. The alignment with the wind is therefore fully dependent on the yaw moment of rotor and tower while no active yaw control is needed. The main engineering challenge in the design of passively yawing FOWTs is to keep the yaw misalignment angle as small as possible. This angle results from the balance of hydrodynamic and aerodynamic yaw moments in various environmental conditions. Consequently, the exact determination of the rotor yaw moment is a crucial part of the design process.

Although the need of designers for knowledge about the exact calculation of the yaw moment is significant, experimental and numerical studies are very rare. This is especially true when considering a downwind rotor with moderate to high cone angle, which is a favourable design for passively yawing FOWT due to its significantly higher yaw moment. As a result, it is unclear if the state-of-the-art design methods for wind turbine aerodynamics are capable of predicting the rotor yaw moment correctly. Therefore, this work aims at gaining a deeper insight into the prediction of the yaw moment of a downwind coned wind turbine rotor. The investigation is based on a detailed experimental study conducted in the wind tunnel of the Hamburg University of Technology (TUHH). The state-of-the-art Blade Element Momentum Theory (BEMT) method AeroDyn v15,[1] the Reynolds Averaged Navies Stokes (RANS) solver ANSYS CFX and the wind tunnel measurements are used to determine the yaw moment of the model turbine with a 5° downwind cone angle at a large number of different yaw angles between -55° and 55°. In order to account for a realistic wake skew angle in the BEMT simulations, the frequently used wake skew correction method based on the work of Pitt and Peters[2] is applied and a parameter study is performed. It is demonstrated that the Pitt and Peters correction method is not capable of improving the prediction of the yaw moment in this case and the direct influence of the correction on the mean yaw moment is analysed. The aim of the RANS simulations is the investigation of the influence of the lateral force on nacelle and blades on the measurement of the rotor yaw moment. Based on these results, a correction of the measurements, which allows for a subsequent translation of the measurement position into the rotor centre, is presented. Finally, an analysis of the measurement uncertainty is performed to give the reader a clear basis to evaluate the results of this study.

The next four sections provide a view on the physical aspects related to the yaw moment and a discussion on the simulation results of wind turbine rotors in yawed inflow using BEMT methods including corrections and RANS methods. Furthermore, relevant experimental studies are described and the conducted experimental investigation is placed into its context. In Sections 6 and 7 experimental and numerical results are compared and analysed followed by a summary of the most important conclusions drawn from the conducted study.

2 | YAW MOMENT AND CONE ANGLE

The yaw moment has not been in the focus of the wind turbine research activities in the past. Therefore, the discussion on the underlying effects had a limited level of detail. Nevertheless, two effects are presented in recent literature: First, Haans[3,4] claimed that the induced axial velocity of the wake on the downwind side of a rotor under yawed inflow condition is higher than on the upwind side. He concluded that the difference in axial induction is caused by the average shorter distance between a given blade section and the tip vortices. A sketch and a visualisation of the tip vortex geometry in yawed inflow are given in Figures 1 and 2. This explanation is justified with observations from hot-film Constant Temperature Anemometry measurements and smoke visualisations of the tip vortices in the wake of a model wind turbine in yaw. Subsequently, a blade on the downwind side of the rotor experiences a lower thrust force. This imbalance of thrust between the upwind and the downwind side causes a stabilising yaw moment in uniform inflow, which means that the yaw moment supports the realignment of the rotor with the wind. Schepers[5,6] confirmed this hypothesis in different studies of the JOULE Dynamic Inflow, MEXICO and NASA-Ames wind turbine experiments.

[*] https://www.equinor.com/en/what-we-do/floating-wind.html.
[†] https://www.aerodyn-engineering.com/downloads/data-sheets/.
[‡] https://www.inocean.no/projects/sway-offshore-wind-turbine/.
[§] https://www.x1wind.com/
[¶] https://www.eolink.fr/.
[#] https://www.cruse-offshore.de/.

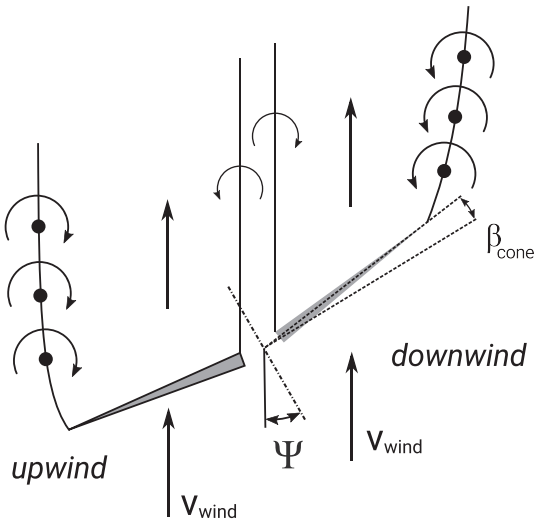

FIGURE 1 Sketch of a typical wind turbine wake under yawed conditions (adapted from Haans3 and slightly modified)

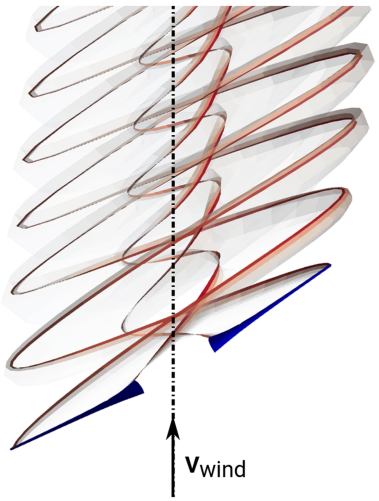

FIGURE 2 Wake visualisation of a two-bladed model turbine in yawed inflow computed by the free vortex wake boundary element method *pan*MARE.[8] Blades are coloured blue, trailing vortices in red

The second effect contributing to the yaw moment is the influence of the cone angle, which is indicated in Figure 1. Due to the slightly different angles between the blade axis and the inflow velocity v_{wind} on the upwind and on the downwind side, another imbalance in thrust occurs and causes a stabilising yaw moment when a downwind cone angle is applied.

As a consequence of the two above-mentioned effects, the local angle of attack (AoA) varies during one rotation. Both effects, downwind cone angle and unbalanced induction on the upwind and downwind side, cause an oscillation of the local AoA, which is maximum on the upwind side and minimum on the downwind side, that is, when the blade is in a horizontal position as shown in Figure 1. This oscillation leads to a hysteresis effect of the lift and drag forces on the airfoil sections,[5,7] which creates a time lag so that the maximum axial and tangential loads on the blade sections occur slightly delayed.

In addition to this, the advancing and retarding blade effect (see Schepers[6]) is present during operation in yawed inflow. An oscillation of local AoA and local inflow velocity is caused by the varying contribution of the yawed inflow to the local inflow velocity in tangential direction. Here, the local inflow velocity in tangential direction at the blade is minimum when the blade crosses from the upwind to the downwind side of the rotor and maximum when it crosses from the downwind to the upwind side, that is, when the blade is in a vertical position. The tangential inflow velocity oscillates while the axial inflow velocity remains constant, which results in an oscillation of the local AoA. As the local AoA and inflow velocity are equal on the upwind and the downwind side when the blade is in a horizontal position, theoretically no contribution to the yaw moment is expected from the advancing and retarding blade effect. However, when additionally considering a time lag in the lift and drag forces

due to the dynamic change of AoA and tangential inflow velocity, the maximum and minimum blade loads arising from this effect occur slightly delayed yielding a small contribution to the yaw moment.

Depending on the operation conditions and the turbine design there are a number of other effects that may also influence the yaw moment: A tilt angle, wind shear and the flow field of a tower near the rotor lead to a velocity deficit in the lower half of the rotor plane, which may cause a yaw moment due to hysteresis effects or asymmetry. Strong fluctuation and hysteresis of lift and drag due to dynamic stall may also alter the yaw moment. At high yaw angles, the tip vortices on the downwind side of the rotor may be convected downstream very slow due to the strong local axial induction. In this case, the presence of wind turbulence may also have an important influence on how the tip vortex positions change over time and how the yaw moment behaves in this region of operation. However, as these and the afore mentioned effects may counteract each other, a distinction between their contributions to the yaw moment is difficult. In order to provide a distinct data set for the validation of numerical methods, a turbine model was developed in such a way that the effect of cone angle and imbalanced axial induction due to the wake contribute most to the generation of the yaw moment. Therefore, the ability of numerical methods to model the basic phenomena of yaw moment generation can be validated with the obtained experimental results.

3 | NUMERICAL METHODS

In the following section, an overview over the utilised numerical methods and their application to wind turbine rotors in yawed inflow is given. This is followed by a description and discussion of the model setups and corrections for the BEMT and RANS simulations.

3.1 | BEMT and yawed inflow

The validity of the classical BEMT for yawed inflow condition is limited as it assumes that the induction due to the wake can be modelled with independent annular rings. The azimuthally varying induction caused by an imperfect wake geometry, a skew angle of the wake, which is not necessarily equal to the yaw angle, and a varying strength of the wake vortices fundamentally contradict this assumption. To overcome this issue and in attempt to incorporate the influence of the skewed wake on the axial induction, a number of correction methods were developed. Here, only a brief summary is given, as a more elaborated description of these attempts can be found in Micallef and Sant.[9] Most of the wake skew correction methods are based on the idea of Glauert, who introduced a sinusoidal variation of the axial induction a_{yaw} with the azimuth angle ϕ:

$$a_{yaw} = a\left(1 + K\frac{r}{R}sin\phi\right). \tag{1}$$

Where a is the mean axial induction from the BEMT iteration and $\frac{r}{R}$ denotes the relative radius of the radial section under consideration. The oscillation's amplitude can then be determined by the factor K, for which Pitt and Peters[2] proposed a formulation based on the wake skew angle χ.

$$K = \frac{15\pi}{32}tan\left(\frac{\chi}{2}\right) \tag{2}$$

$$\chi = (0.6a + 1)\chi_0 \tag{3}$$

The skew angle can be computed using the approximation from Burton[10] in Equation (3), where χ_0 represents the yaw angle. This and other models for example by Coleman[11] or White and Blake[12] for the factor K can be approximated with a linear function up to 40° and therefore mainly vary in the slope of the K-function. Schepers summarised the observations of multiple wind tunnel measurements focusing on the variation of the axial induction in yawed inflow in Schepers.[6] It could be shown that the root vortices have significant influence on the load variations at the inner part of the blade, which is neglected by the correction methods based on Glauert's idea. To account for the root vortices, Schepers developed a more elaborated model, which is based on a second order Fourier series fit of wind tunnel measurements. A validation study[13] was conducted with measurements from the NREL UAE Phase VI Experiment,[14] and it was shown that the model was able to improve the prediction of the unsteady blade loads at the inner blade part. Nevertheless, the mean yaw moment was overpredicted especially near the tip. However, this model is not used frequently in the scientific community and therefore this study utilises a Glauert-based model or—to be more precise—the Pitt and Peters model.

The factor $15\pi/32$ in Equation (2) was discussed by several researchers[10,15,16] ranging from $15\pi/64$ to $15\pi/32$. Which is, when considering the above-mentioned linear K-function instead of the $tan\left(\frac{\chi}{2}\right)$ term, a discussion on the slope of the oscillation amplitude with the rotor azimuth angle. As no best practise was developed in literature, a parameter study on the influence of this factor on the mean yaw moment is presented later in this work.

3.2 | BEMT simulation parameters

All simulations were conducted using the state-of-the-art BEMT method AeroDyn v15,[1] which was developed by the National Renewable Energy Laboratory (NREL). As stated above, the Pitt and Peters wake skew correction was utilised. Further details on the implementation of this model can be found in previous studies.[15,17] Tip and hub loss corrections based on Prantl[1] as well as tangential induction were included in the simulations. With regard to the oscillations of AoA and local inflow velocity described in Section 2, there is a need for a model that takes unsteady airfoil aerodynamics, that is, hysteresis effects on lift and drag into account.[7] In AeroDyn v15, a slightly modified Beddoes-Leishman model[17] is implemented, which is able to model the time lag in the response of lift and drag forces due to a sudden change of the AoA. This time delay results in a phase shift between the sinusoidal variation of the blade loads and the AoA caused by the advancing and retarding blade effect. Therefore, maximum and minimum blade loads do not occur exactly at an azimuth angle of 0° or 180° but are shifted to one side of the rotor, which leads to a contribution to the yaw moment. The same is true for the sinusoidal variation of the local inflow velocity due to the advancing and retarding blade effect. However, in AeroDyn v15, the unsteady aerodynamics model does not consider changes in the local inflow velocity in terms of a time lag of the blade loads. As both effects contribute to the yaw moment in opposite directions (when a blade passes from the downwind to the upwind side, the AoA decreases while the local inflow velocity increases), modelling only one of them results in an insufficient contribution of the advancing and retarding blade effect to the mean yaw moment. Therefore, the unsteady aerodynamics module is not used in the simulations to be able to evaluate the utilised wake skew model. As the distance between rotor and tower was chosen as large as possible, no measurable tower shadow effect is expected (see Section 5). Therefore, no tower shadow model is utilised in the simulations.

3.3 | Application of RANS methods for wind turbine rotors

RANS methods have been applied and validated for the prediction of the flow field around and the loads on wind turbine rotors in many cases, for example, previous studies,[18,19] and proved to model the relevant fluid dynamic phenomena sufficiently accurately, when suitable models and parameters were applied. However, the accuracy of RANS methods using standard two-equation turbulence models suffers from numerical diffusion effects, which may influence the flow field in the mid and far wake.[20] As the numerical simulations are used to determine the loads on blades and nacelle, the choice of the turbulence model was inspired by the results of a code-to-code and code-to-experiment comparison of a similar model wind turbine led by Krogstad,[21] where torque and thrust were measured accurately. In the comparison, several computational fluid dynamics (CFD) codes were used to compute torque, thrust and flow velocities in a certain distance behind of the model rotor in various operation conditions. Most codes showed a reasonable agreement with the measured loads near the optimal operation conditions, while a broader spreading of results for the velocities in the wake can be observed between the codes. Still, none of the methods turned out to perform significantly better than the others. In the present study, the $k-\omega$ SST model is utilised because of its robustness.

When comparing the results of a fully turbulent simulation with those of a laminar-turbulent transition flow simulation, Zhang et al[22] reported a consistent difference in torque and thrust acting on the MEXICO rotor. This indicates that a laminar-turbulent transition needs to be considered when focusing on the blade loads and the presence of such transition on the blade surface cannot be excluded empirically.

3.4 | RANS modelling approach

RANS simulations were performed using the commercially available solver ANSYS CFX and a second order upwind scheme was applied. Preliminary 2D simulations of the wind turbine airfoil utilising the transitional SST ($\gamma - Re_\theta$) model[23] showed that a laminar-turbulent transition occurs on the pressure and suction side of the airfoil at the expected operation conditions of the model rotor. Therefore, the 3D transitional SST model was also applied in the 3D simulations of the present model rotor (see Figure 3). The rectangular far field domain with a width of 70 rotor diameters (D), a height of 50 D and a length of 80 D is discretised comparatively coarse. A sphere is placed inside the far field, which is utilised to apply the yaw angle. Inside the sphere, a rotating cylindrical grid contains the two rotor blades. The composition of the grid is illustrated in Figure 4. The rotor blade is modelled with an O-grid topology. In order to resolve the boundary layer flow y+ is kept below and near one. For an inflow with 55° yaw angle, a grid study with 3.4, 5.0, 7.0 and 9.2 million cells and a temporal discretisation of 4° azimuthal rotation per time step was performed. Torque and thrust of the rotor show an asymptotic behaviour. The grid with 5.0 million cells gives a maximum deviation of 1.5% in torque and thrust compared to the finest grid and was therefore chosen as a trade-off between computational time and accuracy. The results show that the chordwise discretisation in coarse mesh with 3.4 million cells is too low to capture the transition point accurately, which lead to a rapid increase of the discretisation error. Figure 5 shows the surface grid on one blade while a cut through the volume grid near the blade is illustrated in Figure 6. The simulation results for a range of yaw angles are shown in Section 6.

FIGURE 3 Wind turbine model in the wind tunnel

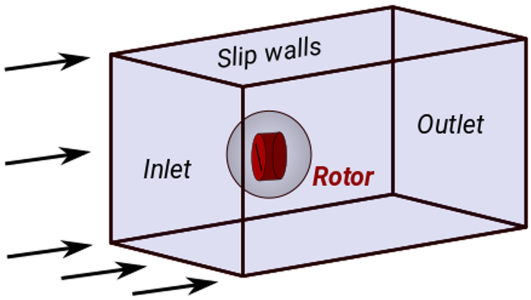

FIGURE 4 Sketch of grid topology for RANS simulations. Dimensions not true to scale

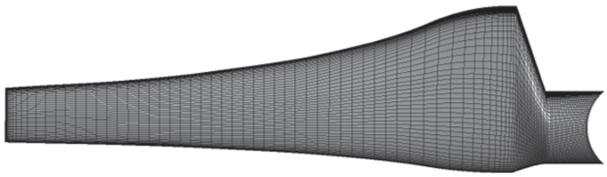

FIGURE 5 Spatial discretisation of the blade surface

4 | PREVIOUS EXPERIMENTAL INVESTIGATIONS

A considerable number of wind turbine experiments in yawed inflow have been conducted in the past 40 years. However, only few of them investigated the yaw moment. Micallef and Sant[9] have provided an overview on the research and most of the relevant experimental studies in this field going back to 1982. Another review of wind turbine experiments including yawed inflow has been presented by Schepers and Schreck.[24] Performing reliable and well calibrated load measurements on full scale wind turbines in yaw is a challenging task and therefore, such investigations are rare. Nevertheless, some elaborate investigations monitoring the blade loads in yaw (e.g. Tjæreborg[25] and DanAero[26]) have been carried out. However, in these experiments, a large number of external influences like wind shear, fluctuating wind, blade and tower flexibility as well as a considerable amount of uncertainty on the turbine and the environmental conditions are present. In contrast to this, wind tunnel experiments can exclude most of these influences, which may superimpose the basic physical effects described in the previous section and therefore seem to be more appropriate to investigate these in detail. Most of the studies in wind tunnels analysed the flow field in the wake or at the tip in order to understand the physics of a yawed inflow.[27–29] Consequently, not all investigations have monitored the loads on the rotor. A brief description of the relevant experiments allowing a determination of the yaw moment due to their measurement apparatus is given in this section.

Krogstad[30] and Lund analysed the aerodynamic loads acting on a wind turbine model with a rotor diameter of 0.9 m. The robust design of tower and nacelle allowed for a comparatively high rotor speed and therefore the aerodynamic behaviour of the rotor could be investigated in a

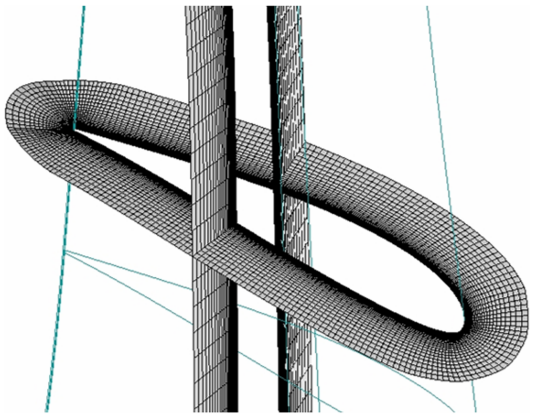

FIGURE 6 Orthogonal cuts through the volume grid near a blade

wide range of tip speed ratios (TSR). A Reynolds number of approximately 1×10^5 was reached at the optimum TSR of 6 and the highest applied wind speed. Measurements with a slightly lower wind speed (leading to a lower Reynolds number) showed only minor changes in power and thrust coefficients at the optimum TSR. Applying even lower wind speeds resulting in a Reynolds number of approximately 0.8×10^5 and lower led to a significant decrease of the maximum power coefficient. This indicates that for the used NREL S826 airfoil, a Reynolds number of 1×10^5 is closely sufficient to maintain a low dependency of the measurements on changes in the Reynolds number. Measurements were carried out using a torque transducer in the nacelle and a six-component balance located below the wind tunnel floor. As the thrust force could only be measured by the six-component balance, an additional test was conducted without the blades to investigate the contribution of the drag force acting on the comparatively large tower and nacelle, and the results were used to correct the thrust.[31] This procedure leads to uncertainties in the thrust measurement as the influence of the velocity deficit in the wake of the rotor on the tower loads is not considered. Krogstad and Adaramola[31] used the same setup to investigate torque, thrust and wake behaviour of the rotor at yaw angles up to 50° in 5° and 10° steps. A considerable effort was made to cover the full operating range of the rotor with tip speed ratios from 0.5 to 12 at every yaw angle. In a later test series conducted by Bracchi[32] and Krogstad, the yaw moment was investigated at three different yaw angles up to 30° in upwind and downwind configuration. The yaw moment was measured by the six-component balance and again corrected with measurements in parked conditions. The obtained results generally show a non-smooth behaviour and large discrepancies are observed when comparing the yaw moment at negative and positive yaw angles. Bracchi et al. mentioned that the correction applied to the measured yaw moment reached up to 70% of the actual value and therefore may cause the inaccuracies. In another study, Bartl[33] used the same turbine to investigate the loads on a wind turbine rotor in the wake of another one. During this campaign, the yaw moment was also measured using the underfloor balance; however, the results were not corrected and therefore contain a considerable amount of the drag loads on the comparably big nacelle and tower.

Maeda et al[34] conducted an experimental study using a model turbine with 2.4 m rotor diameter that focused on blade pressure measurements and additionally recorded the torque using a non-specified 'torque meter'. Thrust and yaw moment could therefore be obtained from the local blade pressure measurements but were neither computed nor published for this experiment.

As mentioned above, the investigation of the yaw moment was also part of the EU JOULE 1 project,[35] where yaw angles of 0°, 10°, 20°, and 30° were applied. A comparatively high Reynolds number of approximately 2.4×10^5 was reached with a rotor diameter of 1.2 m, while the blockage ratio was about 28% in exchange. The focus of the experiments lay on the azimuthal variation of the yaw moment, while the absolute value of the yaw angle may be overpredicted due to the high blockage ratio.

More recent works by Verelst et al[36–38] focused on the dynamic behaviour of a free yawing downwind model turbine. The blade loads were measured using strain gauges at the blade root, but suffered from a high repetition error. While a number of blades with varying sweep were built, no downwind cone angle was applied.

Three different cone angles in upwind and downwind configuration were considered in water tank experiments by Kress et al.[39] Similar to the present work, special attention was paid to the yaw moment, which was investigated at -10°, 0° and 10°. In addition to the cone angle, a tilt angle of 8° was applied in order to account for its effect on the yaw moment simultaneously. With a rotor diameter of 0.5 m and a tank cross section of 1×1 m, a blockage ratio of slightly above 19% results. With regard to a 'solidity ratio' of 3%, no blockage correction was applied. The Reynolds number reached approximately 1.1×10^5 at the optimum TSR of 8.4. Strain gauges inside the hollow rotor shaft were used to measure the torque. The yaw moment was measured using different patterns of strain gauges at the tower root and then corrected using measurements of tower and nacelle without blades, similar to the method proposed by Krogstad and Bracchi.[32] The accuracy of this method in combination with the massive size of the nacelle in comparison to the rotor swept area was not investigated in this specific work.

The Nasa-Ames and MEXICO experiments are unique in terms of their small scaling ratio and elaborate testing methodology. In both experiments, measurements from a high number of pressure sensors distributed along the blade surface gave fundamental insight into the flow field around wind turbine blades in yawed inflow condition. In combination with additional velocity and particle image velocimetry measurements (MEXICO), a valuable contribution to the understanding of the yaw moment was made. Thrust and yaw moment could be computed from an interpolation of the pressure loads at different blade sections. However, a particular uncertainty arises from this interpolation, which is analysed by Schepers.[5] Additionally, both turbines were equipped with strain gauges mounted on the cylindrical part of the blade root,[14,40] which were used to measure the blade loads as well as torque and yaw moment. The strain gauges were calibrated; however, due to the use of a single cylinder as a bending beam in two directions, the uncertainties arising from crosstalk are expected to be comparatively high. The MEXICO rotor was mounted on a supplementary six-component balance, which allowed for measuring the combined loads on tower, nacelle and rotor.

Considering the above-mentioned studies, only the Nasa-Ames and MEXICO experiments deliver accurate measurement data for the absolute yaw moment in an essential range of yaw angles. However, a downwind cone angle was only applied in the Nasa-Ames experiment. Being at 3.4° , the cone angle was in a moderate range, so that a positive effect on the restoring yaw moment was limited, however probably measurable. Measurements at 0° , 10° , 20° , 45° and 90° yaw angle were conducted and therefore a coarse picture of power, thrust and yaw moment of a downwind coned rotor could be drawn from the measurements. The measured yaw moment was shortly mentioned in the work of Schepers.[5] Nevertheless, to the best knowledge of the authors, a comprehensive investigation focusing on the yaw moment was not published in the past.

The present study focuses on the two main contributions to the yaw moment, which are the wake-induced imbalance in thrust and the effect of the downwind cone angle (both described in Section 2). In contrast to this, the Nasa-Ames experiment includes more complex phenomena, which are difficult to analyse separately. One of them is the presence of the tower close to the rotor, which introduces a strong asymmetry to the flow field. Another phenomenon is a laminar separation bubble, which is present on a large area of the blade during normal operation.[41] It is unclear how lift and drag of the blades are influenced by this separation when undergoing the above mentioned oscillation of the AoA. Therefore, the rotor under investigation in the present study was designed to maintain attached flow conditions over the whole blade and a comparably simple geometry which results in a well defined flow field with a minimum of disturbances. In addition to this, a downwind cone angle of 5° was applied in order to observe a more distinct effect on yaw moment in comparison to the Nasa-Ames experiment.

5 | EXPERIMENTAL SETUP

The model tests were conducted in the wind tunnel of the Hamburg University of Technology. The wind tunnel's open test section is 2 m in height and 3 m in width and the turbulence intensity is maintained below 0.5%. In order to keep blockage effects on the measurements small, a rotor diameter of 0.925 m and a blockage ratio of 11.2% were chosen. Values of the blockage vary in a range from 17.6% for the MEXICO rotor where blockage effects were present, albeit limited,[40] and 8.8% for the NASA-Ames Experiment where blockage effects were found to be negligible.[42,43] Following Krogstad and Lund,[30] it is assumed that a blockage ratio slightly higher than in the NASA-Ames experiment will still have a very limited impact on the measured quantities at moderate thrust coefficients. The reference wind speed was measured around 5 rotor diameters upstream of the test section using a Prantl probe near the wall but outside the wall boundary layer. A downwind cone angle of 5° was applied to achieve a high yaw moment while staying within the limitations of a realistic commercial design. A two-bladed configuration was used instead of a three-bladed, which leads to a higher local chord length and therefore to a higher local Reynolds number at the blade sections.

5.1 | Blade design and manufacturing

The design driving goals of the blade geometry were aimed at achieving a low sensitivity to changes in the Reynolds number and a high peak power coefficient in order to mitigate fluctuating forces due to viscous effects and achieve realistic operation conditions. On the one hand, a high rotational speed ensures a high Reynolds number and thus low sensitivity to local variations of the Reynolds number. On the other hand, high centrifugal loads due to the rotational speed lead to a flapwise blade bending moment when considering a coned rotor. Therefore, the selection of the used airfoil and the rotational speed of the rotor was driven by a compromise between airfoil thickness, which strongly influences the occurrence, and strength of undesired viscous phenomena, such as skin friction and stall, and the Reynolds number. The SD7062 airfoil meets these requirements, as its thickness is 14% and the drag coefficient as well as its sensitivity to changes in the Reynolds number is comparatively low. Additionally, a detailed experimental study on the aerodynamic behaviour of the SD7062 at appropriate Reynolds numbers is available[44] and a good match with coupled viscous/inviscid boundary layer simulations (e.g. Xfoil[45]) is given. In order to model a finite thickness at the trailing edge, the airfoil was cut at 96% of the chord length and then scaled to the original chord length again (see Figure 7). To avoid undefined airfoil shapes due to a transition between different airfoil geometries, only one airfoil shape is used over the blade radius. Similarly, the distributions of the chord length and twist (see Table A1) form a compromise between a possibly high chord length, which directly contributes to the Reynolds number, and a high lift to drag ratio, which is necessary to achieve a high power coefficient. The considerations above lead to a rated rotational

speed of 1200 RPM, a rated tip speed ratio of 6.25 and a local Reynolds number of 1.5×10^5 at the tip. Figure 3 shows a photograph of the blades mounted on the turbine. The local Reynolds number, which is calculated based on the free stream velocity and rotational speed, is maintained but decreases slightly down to 30% of the rotor radius and falls to 1.0×10^5 in the root region (see Figure 8). As a result, comparatively low changes in the viscous boundary layer and therefore a straightforward calibration of lift and drag coefficients for simulation methods is expected. However, due to the fact that the local Reynolds number is around two orders of magnitude smaller compared to a full scale turbine, scaling effects need to be considered when transferring the results of the analysis. The main driver of such scale effects is the viscous boundary layer on the blade surface, which causes a slight decrease of the lift and a strong increase of the drag forces acting on the blades at low Reynolds numbers. As discussed in Section 2, the yaw moment can be understood as an imbalance of the thrust force between the upwind and the downwind side of the rotor. Therefore, the increased drag forces are expected to have minor influence on this quantity. In contrast to this, the reduced lift forces may lead to a lower induction and alter thrust force and yaw moment. In order to keep this effect as small as possible, the above mentioned airfoil, which was developed for low Reynolds numbers, has been chosen. In sum, scaling effects may alter the level of the measured forces causing the yaw moment, while only minor influence on the development of the yaw moment with the yaw angle is expected.

The rotation of the blades in combination with the cone angle induce extreme accelerations on the structure: At 0.5 R (radius), approximately 30 times the gravitational acceleration acts on the blade in the flapwise direction. To withstand the extreme loads caused by the accelerations, the blades were manufactured from a carbon fibre prepreg material, as an extremely lightweight and rigid material was required. A CNC-milled hard resistance foam core and a prepreg shear web were inserted into the blade and tempered together with the hull in an aluminium mould. Additionally, an aluminium inlay with threads was inserted at the blade root and aligned in the mould. Due to the high risk of undesired twisting, which may occur from the heating of the anisotropic material, it was necessary to conduct a 3D scan of the blades. The 3D scan was carried out using a laser line scanner mounted on an 8-axis measurement arm. Both blades showed a twist deviation below 0.2° from the original model. The accuracy of the method is estimated to be 0.1°. Additionally, a warp in flapwise direction occurred with a magnitude below 0.3% of the blade length at the blade tip. Figure 9 shows the deviation of the measured blade axis from the original in flapwise direction (triangles) of one blade. Due to its nearly linear shape, it can be interpreted as a deviation of the cone angle of approximately 0.1°. In order to account for the inertial loads, a second 3D scan was conducted under equivalent operational loads using two 2 kg weights. The additional blade bending is plotted with circle symbols in Figure 9. No significant bend-twist coupling was observed when applying the weights. While small deviations in power and

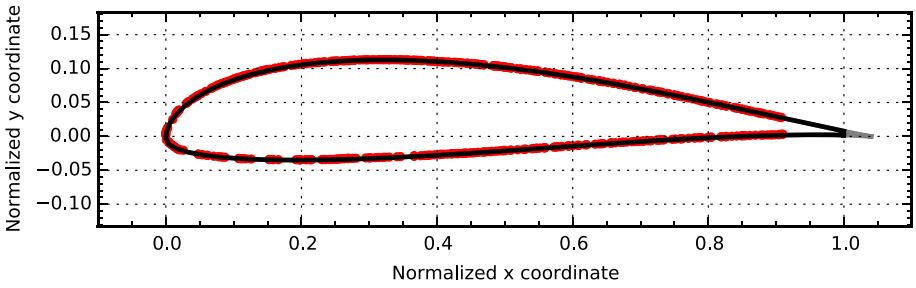

FIGURE 7 Geometry of SD7062 airfoil with cut trailing edge. Red dots indicate results from 3D measurement. Coordinates were normalised to a chord length of 1

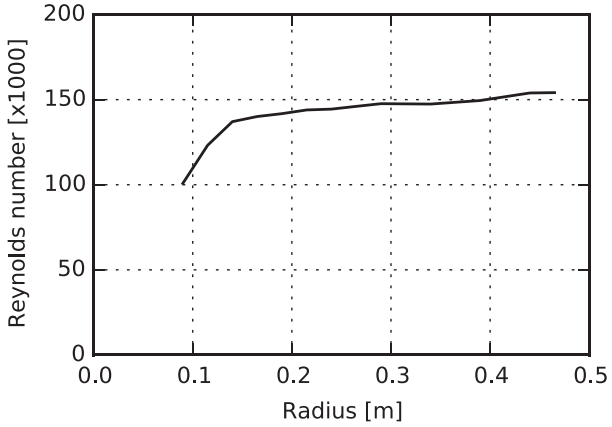

FIGURE 8 Local Reynolds number at the blade sections over rotor radius

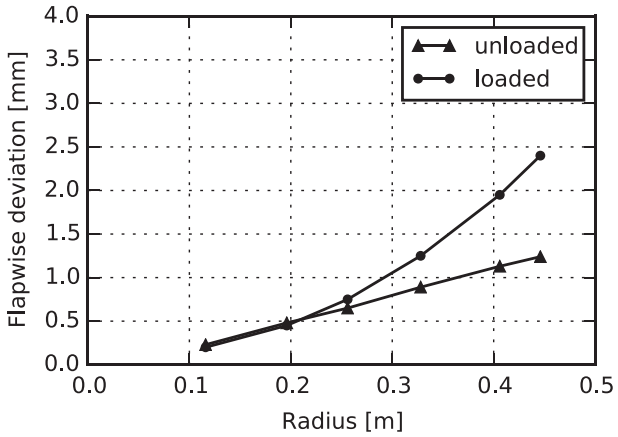

FIGURE 9 Deviation of measured blade section midpoint to design blade axis in flapwise direction

thrust are expected as a result of the twist deviation, it is assumed that the bending does not have a measurable influence. An exemplary radial cut of the scanned 3D point cloud (red dots) and the CAD geometry of the blade (black line) is illustrated in Figure 7, where the deviations in blade axis position and twist angle were compensated. As the laser line scanning method is not suitable for sharp edges, the trailing edge (TE) is not resolved in Figure 7. It can be observed that the scanned points match very well with the intended airfoil contour. The deviations of the wind tunnel model from the original rotor geometry are summarised in Table 1. The blade manufacturing was supported by Cruse Offshore GmbH.

5.2 | Mechanics and instrumentation

The 5-axis CNC-milled aluminium hub is mounted on a steel shaft and can be turned around to enable an upwind cone angle. Both blades can rotate around the blade axis due to a cross roller bearing at the blade root and a pitch mechanism, which is not in use in this work. Therefore, the pitch angle is adjusted manually. It is assumed that the deviation of the zero pitch angle can be kept below 0.3° using a calibration gauge. A Kollmorgen TBMS-6051 brushless DC motor with a maximum continuous torque of 1.16N m is mounted at the end of the main bearing housing. The constant rotational speed is maintained by a digitally adjusted load resistor connected to the motor. All force and moment measurements are undertaken with a ME-Meßsysteme KD40 six-component load cell mounted below the main bearing housing. The calibration of the sensor was carried out with 12 different load vectors in the operation space to consider the effects of cross talking, as not only the aerodynamic loads but also loads due to a small rotor imbalance occurred. The analysis of the calibration results shows that the expectable measurement uncertainty is 0.128N in thrust, 0.024N m in torque, 0.008N m in yaw moment and 0.024N in lateral force (with a confidence level of 95%). In relation to the loads at rated conditions, a measurement uncertainty of 0.5% in thrust and 2.3% in torque and power is determined.

Different yaw angles from -55° to 55° were adjusted by an underfloor turntable with an uncertainty of below 0.25°. Two steps were conducted for the initial alignment of the 0° position: First, the rotor axis was aligned parallel to the wind tunnel floor using a digital level. Second, the blade tips were aligned with a line laser that projected a plane perpendicular to the wind tunnel floor and inflow direction. Therefore, a maximum yaw angle uncertainty of 0.5° is expected, as the wind tunnel floor cannot be assumed to be perfectly even.

5.3 | Signal processing

All signals measured by the load cell were recorded over time with a sampling frequency of 2.4 kHz and a low pass filter with a corner frequency of 40 Hz was applied. Extreme outliers were removed from the signal using a standard deviation-based filter. Torque, thrust, yaw moment and lateral force were measured directly, whereas the power was calculated from the measured torque and rotational speed. As the native coordinate system of the sensor is positioned on its top, a coordinate transformation was applied. It was translated along the z-axis (perpendicular to the wind tunnel floor), so that the x-axis is equal to the rotor axis pointing in downwind direction (see Figure 10). This transformation is based on the assumption that the lateral force on nacelle and rotor can be described as a single vector whose point of application lies on the rotor axis. This assumption seems reasonable as the nacelle is axisymmetric. A further translation of the coordinate system into the rotor centre O_c is not applicable since the exact point of application of the lateral force in x-direction is unknown. Therefore, the origin of the coordinate system, to which the presented loads refer, is located in a distance $d_{sensor-RC}$ equal to 80.6 mm to the rotor centre in downwind direction, while the x-axis is identical to the rotor axis. Finally, a mean value was calculated for all signals in a window of 1 s, which corresponds to 20 rotor revolutions. Considering the

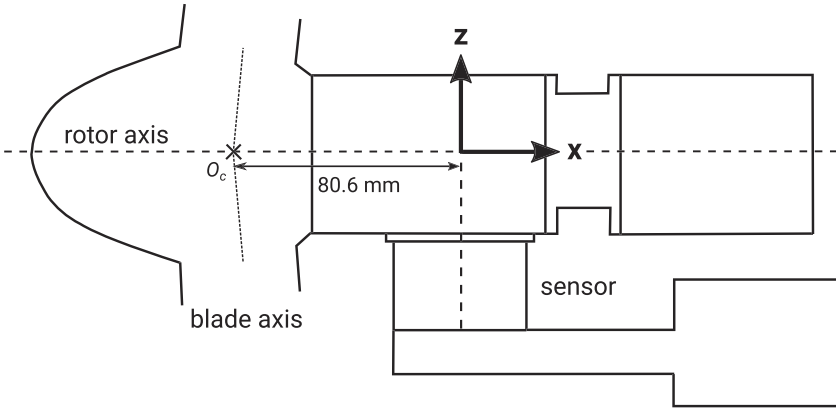

FIGURE 10 Sketch of the model turbine and applied coordinate system

TABLE 1 Geometric uncertainties of the wind tunnel model from the original geometry

Feature	Deviation from CAD model
Blade length	<0.1%
Twist angle	<0.2°
Pitch angle	<0.3°
Chord length	<1%
Local blade shape (excluding TE)	<0.1 mm
Cone angle	<0.2°
Circular runout	<0.05 mm

mean values, the fact that the corner frequency of the low pass filter is equal to the blade frequency does not influence the calculated values. For an evaluation of the measurements in time domain, a higher corner frequency would need to be applied.

6 | RESULTS

Results obtained from measurements, BEMT and RANS simulations for power, thrust and yaw moment coefficient as well as the lateral force of the model turbine at rated conditions (see Table 2) and different yaw angles are shown in Figures 11 and 12. The yaw angles in the experiment range from -55° to 55° and are distributed symmetrically (apart from 3 points missing in the positive and 1 in the negative angle region). Due to power losses in the drivetrain, the rotational speed could not be maintained at yaw angles above 55°. In total, the measurements contain 53 different yaw angles. In the diagrams, black crosses connected with lines indicate the measurement points whereas light blue crosses are obtained by mirroring of the measurement points at the *y*-axis. In case of the yaw moment, the light blue crosses are additionally mirrored around the *x*-axis in order to account for the change of the sign at negative yaw angles. Solid and dash-dotted blue lines illustrate the simulation results computed by the BEMT method AeroDyn v15. For the solid blue line, no wake skew correction was applied, while the results using the factor $15\pi/64$ for the above mentioned K -function are plotted with dash-dotted lines. For the sake of simplicity, the modified wake skew correction models are referred as Pitt and Peters corrections with varied parameters. Connected red triangles indicate the results from the RANS simulations. It has to be noted that sensor and tower (see Figure 10) are neglected in the RANS simulations and the nacelle is slightly modified to achieve a rotational symmetric body.

The power and thrust coefficients C_p and C_t are defined in Equations (4) and (5).

$$C_p = \frac{P_{mech}}{\frac{1}{2}\rho v^3 A_{rotor}} \tag{4}$$

$$C_t = \frac{F_{thrust}}{\frac{1}{2}\rho v^2 A_{rotor}} \tag{5}$$

TABLE 2 Model properties

Rotor diameter	**0.925 m**
Rated wind speed	9.3 m s^{-1}
Rated rotational speed	1200 RPM
Nacelle diameter	72 mm
Tower diameter	57 mm
Distance blade tip to tower	530 mm
Distance rotor centre to coordinate system	80.6 mm
Air density	1.183 kg m^{-3}

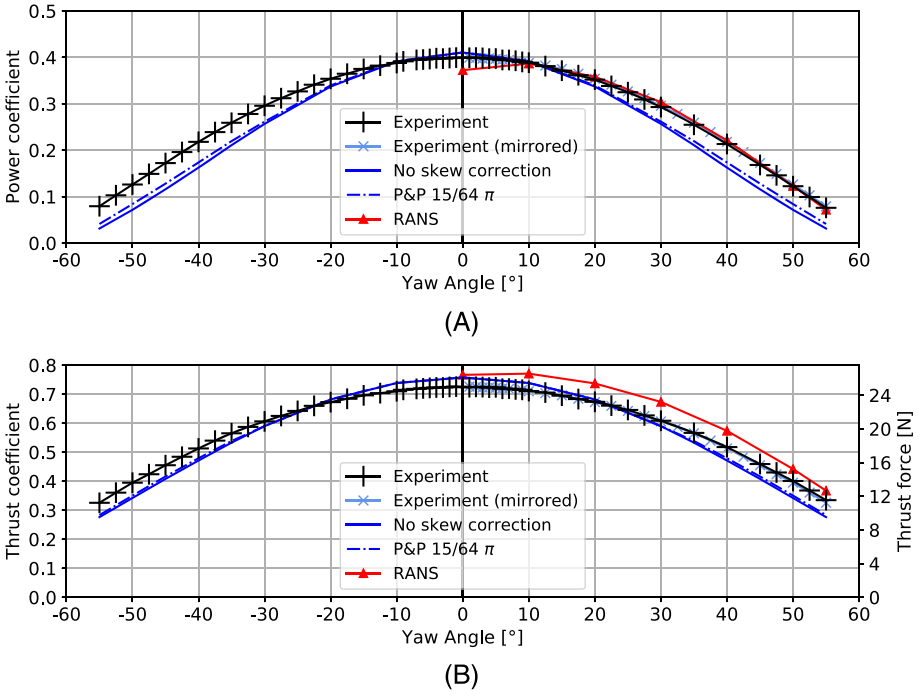

FIGURE 11 Comparison of experimental and numerical results for (A) power coefficient and (B) thrust coefficient over yaw angle

Where P_{mech} and F_{thrust} denote the mechanical power and the thrust force. Air density, wind speed and rotor swept area are described by ρ, v and A_{rotor}, respectively.

Apart from the lateral force, all experimental curves show a very smooth behaviour. When comparing the measurement points of power and thrust coefficients in Figure 11 with their mirror images, the differences are barely visible. This observation demonstrates a high degree of symmetry and meets the expectations regarding the physical behaviour of the rotor. The standard deviations for the case of axial inflow, where all loads are expected to be constant during one rotation, are as follows: 0.0118N m in torque (corresponding to 1.2%), 0.23N in thrust, 0.020N m in yaw moment and 0.15N in lateral force. At small yaw angles, the BEMT simulation results match the measured power coefficient well. With rising yaw angle, an offset develops and stays more or less constant up to the highest yaw angles. However, due to the decreasing level of power, the relative deviation to the measured results reaches more than 40% at 50° yaw angle. A similar trend can be observed in the course of the thrust force, where the decrease of the thrust with the yaw angle is also overestimated. In contrast to the power coefficient, a slight overprediction of the thrust occurs at small yaw angles, which decreases the deviations at higher yaw angles. Only very small differences between the simulations results of power and thrust due to the utilisation of the wake skew model are visible. This is straightforward and meets the expectations as the sinusoidal variation of the axial induction introduced by the Pitt and Peters wake skew model should not have a significant influence on the mean axial induction, which is the driving quantity for mean power and thrust. So far, power and thrust of the model turbine can be captured with a comparatively high accuracy by the AeroDyn simulations. Considering the results of the RANS simulations, the decrease of power at higher yaw angles can be reproduced exactly. However, an underprediction of the power at 0° yaw angle is visible. The investigation of the numerical results of the RANS simulation shows some limitations of the determination of the transition point under this operation condition. The thrust coefficient is consistently overpredicted, but the decrease with the yaw angle is captured well. Finally, the comparison of power and thrust indicates that the numerical models for the wind turbine are set up appropriately.

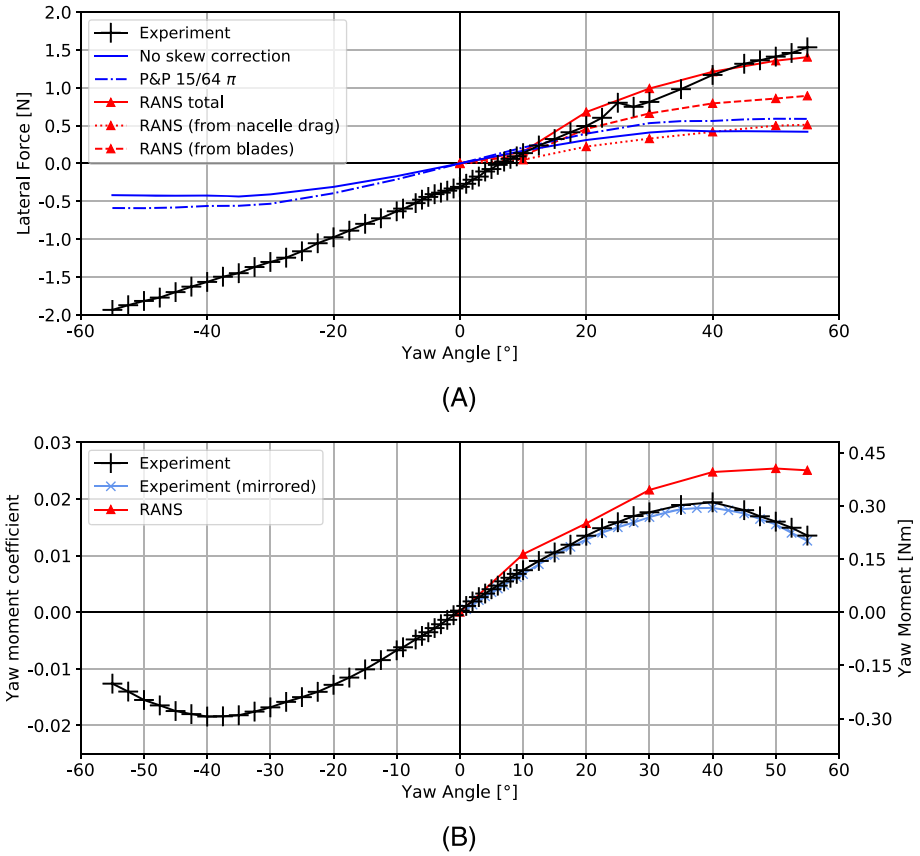

FIGURE 12 Experimental and numerical results for (A) lateral force and (B) yaw moment coefficient over yaw angle

The measured lateral force shown in Figure 12A essentially behaves like a linear function even though the course of the curve is less smooth in comparison to the other quantities. A notable offset of approximately -0.3N from the origin can be observed at 0° yaw angle. In comparison to the thrust force, the lateral force is small, which confirms that the total force acting on the rotor is aligned with the rotor axis, however not with the wind direction—as is sometimes stated in literature. According to the RANS results, the measured forces are a summation of the aerodynamic loads on rotor and nacelle. Taking into account the small magnitude, the overall lateral force predicted by the RANS method can be considered in good agreement with the experiment. From the RANS simulations, the ratio between the contribution from the blades and the nacelle drag to the lateral force could be determined as roughly 2:1. In addition, the resultant force vectors of both forces act approximately in the rotor centre. For the lateral force arising from the blades, this observation is straight forward. However, the overall low contribution and the eccentric point of application of the nacelle drag force was not expected during the planning of the experiment. Considering the instantaneous velocity field on a horizontal plane through the rotor axis in yawed inflow in Figure 13 (top view), an explanation for this behaviour can be found as follows: While a nearly laminar flow developed in the front part of the hub around the stagnation point, the flow around the nacelle near and behind the blade is dominated by the passing hub vortices and therefore fluctuates strongly. This leads to an oscillation of the resulting force around zero, while the force on the front part of the nacelle approximately keeps its direction. Therefore, the mean lateral force on the nacelle originates mostly from the pressure on the hub, which explains its application near the rotor centre.

As the nacelle is not modelled in the BEMT simulations the lateral force is underpredicted. However, when comparing the results of the BEMT simulation (blue curves) with the corresponding values of the RANS simulation (red curves) it is obvious that the lateral force originating from the blade is significantly underpredicted. The influence of the K-factor on the lateral force as well as on mean power and thrust shown in Figure 11 turned out to be marginal. For the sake of readability, only the lowest K-factor (which corresponds to no skew correction) and the highest K-factor are included in the corresponding figures.

In Figure 12B, the yaw moment coefficient C_{ym} and the absolute yaw moment M_{yaw} around the sensor z-axis (see Figure 10) are shown on the primary and secondary y-axis. The yaw moment coefficient is based on the idea of the thrust coefficient and is defined as follows:

$$C_{ym} = \frac{M_{yaw}}{\frac{1}{2}\rho v^2 A_{rotor} R_{rotor}}. \quad (6)$$

Where the rotor radius R_{rotor} refers to the projected blade axis on a plane perpendicular to the rotor axis. Analogous to the thrust coefficient, the denominator forms an ideal reference value, which is defined as the yaw moment arising from the theoretical thrust coefficient of 1 acting at a single blade tip. This definition differs from the suggestion of Kress et al,[39] as their definition depends on the blade surface rather than on the rotor swept area, which does not allow for direct comparison of two different rotor designs with respect to the yaw moment. The measured yaw moment can be described by a linear function with nearly no offset and a slope of approximately 0.011 Nm per degree from -15° to 15°. With increasing yaw angle, the slope decreases until a maximum yaw moment coefficient is reached between 37.5° and 40°. Comparing the measured values with their mirror image around the *y*-axis, higher deviations as observed in torque and thrust occur. A maximum deviation of approximately 4% from the mean of the magnitudes at positive and negative yaw angles is reached at a yaw angle of 27.5°. A reason for this asymmetry could be a misalignment of the zero yaw angle. However, this is not in line with the observation according to which the the yaw moment reaches nearly zero at 0°. As described above, the yaw moment evaluated at the sensor coordinate system is influenced by the nacelle drag force, which is not modelled in the BEMT simulations. Therefore, BEMT results are not shown in Figure 12B.

The findings regarding the application point of the lateral force obtained from the RANS results allow for a correction of the measured yaw moment that suffers from the unfavourable position of the sensor coordinate system: Assuming that the force application point lies in the rotor centre, as shown in the simulations, the yaw moment around *z*-axis in the rotor centre M_{yawRC} can be computed from the measurements as follows:

$$M_{yawRC} = M_{yaw} + F_{lat} * d_{sensor-RC}. \quad (7)$$

Where the yaw moment around the sensor *z*-axis is M_{yaw}, the lateral force is F_{lat} and the distance from the sensor midpoint to the rotor centre in rotor axis direction is $d_{sensor-RC}$. The rotor centre is defined as the intersection of the downwind coned blade axes. It has to be noted that the offset in F_{lat} was eliminated before the correction was applied (see Section 7 for details). Figure 14 shows the corrected experimental results at the rotor centre and those of the BEMT as well as the RANS simulations. The conducted RANS simulations slightly overestimate the corrected measurements and reproduce the behaviour with rising yaw angle accurately. However, the decrease of the yaw moment at higher yaw angles cannot be captured and therefore no clear maximum as it is present in the corrected measurements can be observed. As described in Section 2, the yaw moment is partly caused by the geometric configuration of the up- and downwind blade and the tip and root vortex helices. The variation of the induced velocities on the up- and downwind blade monotonically rises with higher yaw angles. Therefore, from a geometrical point of view, the yaw moment would rise monotonically with increasing yaw angle. However, the loading of the rotor decreases with the projected rotor swept area in wind perpendicular to the wind direction. This in turn reduces the strength of tip and root vortices and consequently the induction. Finally, at very high yaw angles, tip and root vortices have vanishing strength. In consequence, the point of maximum yaw moment is determined by an interaction of these effects. The observed good agreement of the decrease of turbine torque and thrust at higher yaw angles between RANS and experimental results indicates that the decrease of the turbine loading can be captured correctly in this case. A possible explanation for the overprediction of the yaw moment is that the development and interaction of existing and newly generated tip vortices on the downwind side of the rotor is not modelled in sufficient detail at extreme yaw angles.

As shown in Figure 14, it seems surprising that the trend of the yaw moment can be roughly captured by the BEMT method without a wake skew model, as the wake-induced oscillation of the axial induction is not modelled by the method. For rotors with no cone angle, this effect is most significant for the yaw moment. However, in this case, the oscillation of axial inflow velocity from the upwind to the downwind side of the rotor caused by the cone angle significantly affects the calculated yaw moment in AeroDyn. Decreasing the cone angle in the simulations leads to a vanishing yaw moment in this case, which supports the hypothesis that the simulated yaw moment without wake skew correction is caused by the presence of the cone angle. However, it is doubtful if a separation of the azimuthal oscillation of the induction in the wake and the geometric

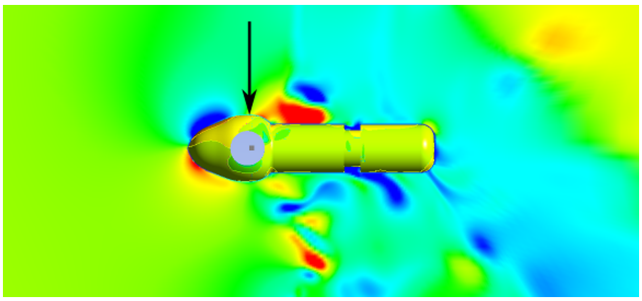

FIGURE 13 Illustration of the velocity field around the nacelle on a horizontal plane (top view). Black arrow indicates the point of application of the resulting force on the nacelle surface

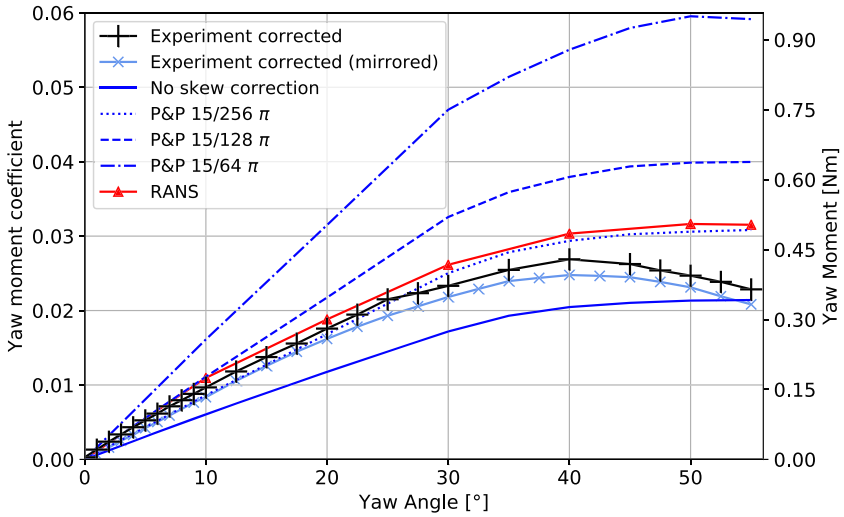

FIGURE 14 Yaw moment coefficient at rotor centre

effect of the cone angle on the local inflow velocity on the blade is valid. It is therefore plausible that a different cone angle would significantly alter the similarity of the AeroDyn results without wake skew correction and experimental results.

The dash-dotted blue line in Figure 14 represents the simulation results of the yaw moment with the Pitt and Peters correction and a factor of $15\pi/64$ applied. It is clearly visible that the yaw moment is overestimated strongly in the whole range of yaw angles. Analogous to the measurements, the shape of the curve initially is linear and flattens at higher yaw angles. This behaviour can be explained by the equations 1 and 2. Taking into account the near-linear behaviour of tangent term up to a wake skew angle of about 50° , it is straight forward that the amplitude of the introduced oscillation of the axial induction a_{yaw} due to the Pitt and Peters model also shows a linear increase at lower yaw angles as the mean induction a decreases slowly in this region. When reaching higher yaw angles, the linear increase is compensated by the strong decrease of the axial induction a. This derivation is based on the assumption that the mean yaw moment is linearly dependent on the oscillation amplitude of a_{yaw}.

As the factor of the K-function was already chosen to be the lower boundary of the discussed values between $32\pi/64$ and $15\pi/64$, it is unexpected that the yaw moment is still overestimated strongly. However, in previous investigations focusing on the blade loads of the experimental turbine in the Nasa-Ames experiments[15,46] it could be observed that the oscillation amplitude of the flapwise blade loads is strongly overestimated by this model, which indicates that this would also be the case for the mean yaw moment. In order to investigate the influence of the K-factor, two more simulation series were conducted testing a half (dashed line) and a quarter (dotted line) of the factor used before. As expected, the yaw moment for those cases decreases over the whole range of yaw angles. According to Equation (2), it is straight forward to see that the oscillation amplitude of the axial induction is linearly dependent on the variation of the factor. As the blade thrust is strongly dependent on the induction, this azimuthal variation of the axial induction causes an imbalance of thrust between the upwind and the downwind blade with a maximum when the rotor is in a horizontal position. Therefore, the yaw moment is directly dependent on the choice of the K-factor, which can also be seen in Figure 14. In consequence, any desired slope of the yaw moment around 0° up to 30° can be tuned in this way.

In summary, the results show that the yaw moment is strongly overpredicted by the choice of any of the factors for the K-function proposed by the mentioned researchers. Tuning of the parameter to match the experimental results up to 40° is possible; however, it remains questionable if a benefit for the simulation of other wind turbine rotors can be achieved. This is due to the fact that there are no definite physical criteria for the selection of the K-factor, which may result in the need to select a different value when certain operating conditions or blade characteristics change. The clear decrease of the measured yaw moment from 40° cannot be reproduced by the Pitt and Peters correction. The reason for this may be the complex wake geometry, which starts to deform more and more from its original helical structure at higher yaw angles. This deformation cannot be taken into account by the BEMT correction model.

7 | DISCUSSION OF UNCERTAINTIES

When interpreting the results of the presented measurement campaign, it is important to note that the experiment was conducted under controlled, albeit not ideal conditions in terms of numerical simulations. This section therefore summarises issues on systematic and random uncertainties in order to provide necessary information for the physical interpretation of the obtained measurements. The influence of misalignments and geometric deviations of the experimental turbine from the computational model discussed in Section 5 are categorised as systematic errors. The latter are assumed to be on a reasonably low level and are not discussed here in detail.

7.1 | Sources of systematic uncertainty

A critical issue for the measurement of the yaw moment is the alignment of the rotor axis with the wind direction. Considering the symmetry of power and thrust with regard to the yaw angle and the zero crossing of the yaw moment, no evidence could be found indicating that the proposed zero yaw angle uncertainty related to the rotor axis is significantly higher than the expected 0.5°. The misalignment of the sensor *x*-axis with the rotor axis can be deduced from the measurement results. In Figure 12A, the offset of the lateral force at zero yaw gives a hint that this adjustment may not be exact. The authors assume that the value measured as the lateral force at 0° yaw angle truly is a fraction of the force in axial direction caused by a misalignment between rotor axis and sensor *x*-axis of approximately 0.7° , which is calculated from the arc tangent of thrust and lateral force. Fortunately, the sensitivity of the measured torque and thrust to small deviations is far below 0.1% due to its correlation with the cosine function at angles near 0°. The yaw moment is not altered by such a misalignment, as it can be interpreted as a rotation of the measurement coordinate system around the yaw axis.

A systematic influence on the corrected measurements of the yaw moment is the uncertainty of the correction method. As the flow field around the nacelle is highly turbulent, it is not clear to which extent the RANS simulations can capture the magnitude, direction and point of application of the nacelle drag force. In contrast to this, the good agreement with the experimental data in torque and thrust indicates that lift and drag forces on the blade sections were computed correctly. As these forces also determine the lateral force originating from the blades, it can be assumed that this lateral force could also be predicted with reasonable accuracy. Therefore, only a small portion of the measured lateral force is dedicated to the nacelle drag force (as shown in Figure 12A), which limits the impact of the above-mentioned potential modelling uncertainties on the correction of the yaw moment. However, the correction induced uncertainty is assumed to be well below 5%; however, no exact upper limit can be given.

7.2 | Sources of random uncertainty

A number of different sources of random uncertainty were observed and their combined influence on the measurement results can be quantified as the repetition error. In addition to the repetition error of the sensor itself, the cables of the generator and rotational speed sensor form a bypass. A change of the forces induced by this bypass, for example, due to vibrations would cause a repetition error. Furthermore, the rotational speed of the model turbine cannot be kept exactly at rated speed. First, the average rotational speed is not exactly 1200 RPM but alters with a maximum of 0.6% from this value. The influence of this effect is considered in the calculation of the power coefficient, while its influence on the aerodynamic flow field contributes to the repetition error. As it is possible to account for the variations in mean rotational speed when using the measurements as a validation data set for simulation, this effect is excluded from this consideration. Second, an oscillation of the rotational speed with an amplitude of approximately 0.25% of the rated rotational speed at its maximum was observed at all yaw angles. Due to the low value, no measurable influence on the uncertainty is expected. In addition to the variations of the rotational speed, the mean wind speed measurement also altered about 0.5% at its maximum. To calculate the power, thrust and yaw moment coefficients, the mean tunnel velocity of 9.3 m s^{-1} was used, which leads to slight deviations in the diagrams. For comparison purposes the actual tunnel speed in addition to the measured absolute values of thrust, torque, yaw moment and lateral force is given in Table A2. Nevertheless, the uncertainty in the measurement of the tunnel wind speed of about 0.05 m s^{-1} contributes to the random uncertainty when considering the load coefficients.

A Fourier analysis of the measured loads in time domain revealed two oscillations that could not be classified as aerodynamic load or dynamic imbalance. One had a frequency of approximately 13 Hz and a maximum amplitude of 0.7N in lateral force. It was classified as the first bending eigenfrequency of the tower by a hammer test. The second was a forced oscillation with angular speed, which appeared in the thrust force with an amplitude A_F of approximately 0.5N. This oscillation was caused by the rotor imbalance acting in circumferential direction. A moment in lateral direction (around the *y*-axis) arose from the imbalance that passed its highest or lowest position. This moment acted as a bending moment on the tower and therefore forced its vibration in wind direction. Both vibrations are therefore caused by acceleration loads due to the nacelle movement in axial and lateral direction. Assuming that the vibrations can be described as a sine function and taking into account the nacelle's mass *m* of approximately 3kg, the velocity amplitude A_v, that is, maximum motion velocity of the tower top in motion direction, can be expressed as follows:

$$A_v = A_a \frac{1}{2\pi f} = \frac{A_F}{m} \frac{1}{2\pi f}, \tag{8}$$

where *f* describes the frequency of the motion, while A_a and A_F stand for the amplitudes of the acceleration and force. For both observed vibrations, the motion velocity does not exceed 0.003 m s^{-1}, which is very small in relation to the inflow velocity. Therefore, no measurable contribution to the uncertainty of the mean aerodynamic loads due to the nacelle motion is considered.

Figures 15 and 16 show the repetition errors of power and thrust measurements during three different test runs (triangles, circles and squares) at three tip speed ratios and a rotational speed of 1200 RPM. At rated conditions, that is, an inflow velocity of 9.3 m s^{-1}, a TSR of 6.25

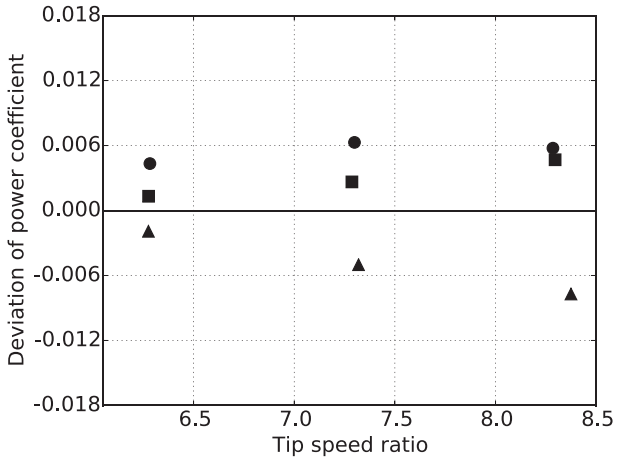

FIGURE 15 Absolute deviation of power coefficient from mean value of three repetitions

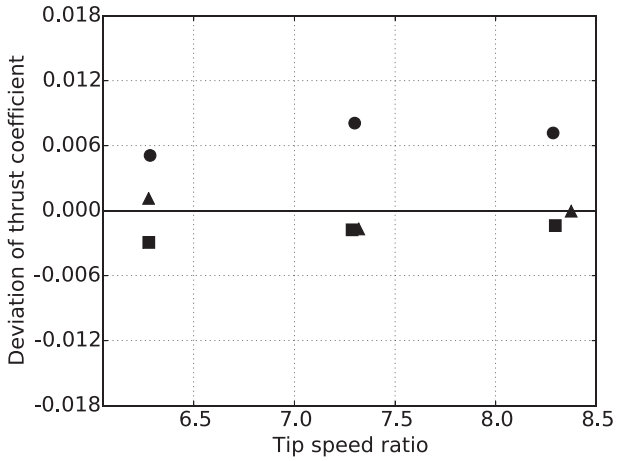

FIGURE 16 Absolute deviation of thrust coefficient from mean value of three repetitions

and zero yaw angle, a repetition error slightly above 1% in power and below 1% in thrust can be determined in this sample. Therefore, the sample shows only half the repetition error of the sensor uncertainty in torque respectively power. As the overall measurement uncertainty in multi-component load cells is mainly driven by cross talking, it is straight forward that the contribution of the repetition error lies below the expected maximum uncertainty when applying a similar load vector. Considering yaw moment and lateral force at rated conditions, the absolute repetition errors in this sample turned out to be 0.005N m and 0.15N, respectively.

8 | SUMMARY AND CONCLUSIONS

In the present study, an experimental and numerical investigation on the yaw moment acting on a downwind coned model wind turbine in oblique inflow is presented. The results gathered during the investigation deliver a more precise understanding of the required modelling fidelity to calculate the yaw moment induced by the yaw misalignment of a wind turbine rotor, which is crucial to determine the restoring moment of a passively yawing FOWT. Passive yaw mechanisms of such FOWT often fully rely on the restoring aerodynamic moment of rotor and other turbine components, so that this moment is a fundamental part of the design. In order to provide an example for the applicability and limitations of state-of-the-art BEMT methods for the design process of passively yawing FOWT, the results of such method were compared to the measured yaw moment. In addition to that, a RANS method was applied to determine the contribution of the lateral force on the measured yaw moment at the sensor position. An experimental setup was developed in order to generate reproducible and accurate validation data in consideration of the following critical aspects: A comparatively high Reynolds number of 1.5×10^5 was reached leading to a low the sensitivity of the results on changes of the Reynolds number and a limited presence of viscous effects. An investigation of the blade geometry and deformation under

approximated equivalent operational loads using a 3D scanning system showed that geometric uncertainties can be considered as negligible. Measurements were conducted using a six-component load cell mounted directly below the nacelle to exclude undesired forces and moments acting on the tower. A detailed analysis of the measurement uncertainty was performed. Furthermore, a correction of the measurements based on the RANS simulations was applied to determine the yaw moment at the rotor centre. Simulations of the measured yaw moment using the BEMT method AeroDyn v15 were carried out with and without the application of the implemented Pitt and Peters wake skew correction, which can be regarded as representative for a number of Glauert-based corrections. To investigate the influence of the Pitt and Peters correction on the mean yaw moment, a parameter variation was performed.

A number of findings regarding the results of the conducted experimental investigation and the uncertainty arising from the numerical prediction of the yaw moment were elaborated:

- The measured aerodynamic loads display symmetric behaviour and a low repetition error, which confirms that the experimental setup was appropriate and a low level of uncertainty could be reached.
- An overall good agreement between RANS simulation results using the transition SST model and the experimental data could be observed. Considering that the absolute value of the lateral force is an order of magnitude smaller in comparison to the rotor thrust force, it could be predicted accurately over all yaw angles. The ability of the RANS method applied to capture the yaw moment at extreme yaw angles proofed to be limited. Therefore, only a rough estimation of the maximum yaw moment and the corresponding yaw angle is possible in this case. A possible explanation for this is that the yaw moment at higher yaw angles is strongly dependent on the interaction of existing and newly generated tip vortices on the downwind side of the rotor, which leads to a strong sensitivity to numerical diffusion and turbulence modelling.
- BEMT method applied was able to capture power and thrust with a comparably low error at low to moderate yaw angles, while deviations up to 40% were observed at yaw angles higher than 40°.
- The application of the Pitt and Peters wake skew correction to the BEMT method led to a strong overprediction of the mean yaw moment when using the parameters proposed in literature. Modifying the parameter opens the possibility to tune the results to the measured yaw moment. However, the benefit of this tuning for the simulation of other wind turbine rotors is limited.
- This overprediction would lead to an overestimation of the restoring moment in the design of passively yawing FOWT, which in turn results in an underestimation of the expected yaw misalignment during operation. As the average power loss due to yaw misalignments is one of the most important characteristics of a passively yawing FOWT design, the usage of the Pitt and Peters model may lead to wrong conclusions on the profitability of a certain design.
- Simulations without wake skew correction delivered a much better prediction of the yaw moment, although only the geometric influence of the downwind cone angle contributed to the yaw moment while important flow features were neglected. It is therefore questionable if such good prediction of the yaw moment can generally be expected for other wind turbine rotors.
- Unsteady hysteresis effects in lift and drag due to the variation of the circulation around the blade were neglected in the simulations as AeroDyn v15 only accounts for changes in circulation due to a variation of the angle of attack. It is, however, unable to take the hysteresis effect of a varying local inflow velocity into account. These effects counteract each other in their influence on the yaw moment initiated by the advancing and retarding blade effect. Therefore, considering only one effect leads to a one-sided distortion of the yaw moment. In total, the influence of the advancing and retarding blade effect on the mean yaw moment is considered to be limited. Nevertheless, simulation results and conclusions need to be interpreted with care, as the hysteresis of lift and drag forces were neglected.
- A positive restoring yaw is maintained over the whole power-producing operation range in experimental and numerical results. The measured yaw moment forms a lying S-shape but can be described as a linear function from -15° to 15°. The decrease of the yaw moment at angles above 40° cannot be predicted by the BEMT and RANS simulations.
- The aerodynamic force on the rotor mainly acts along the rotor axis direction as the measured lateral force is very small in comparison to the axial force. This is in line with previous observations; however, converse statements can also be found in literature.

In addition to the Pitt and Peters model, a number of alternative wake skew correction models for BEMT methods have been proposed in the past. Schepers model[6] seems to be the most promising one. However, in the only known investigation on the mean yaw moment,[5] a significant overestimation was observed. To date, it therefore still remains questionable whether it is possible to apply a BEMT method for the determination of the mean yaw moment of a wind turbine, maintaining a sufficient accuracy for passively yawing FOWT design. Finally, it is recommended to doubt and check the results of BEMT simulations in yaw when the determination of the yaw moment is a crucial part of the analysis. This is of major importance when rotor driven yaw oscillations of FOWT or the functionality of the yaw mechanism of a passively yawing (floating) wind turbine is evaluated. From a physical point of view, free wake methods, which model the axial and tangential induction with discretised vortices in the wake and utilise a lifting line, lifting surface or panel method, are more appropriate for this task. However, only one validation of a lifting-line method in this context is known by the authors, which shows promising results.[5] As shown in this work, CFD methods are also suitable for this task. However, the computational effort usually prevents from using these methods for coupled wind turbine simulations.

Future work should therefore focus on the validation of free vortex wake methods with regard to the prediction of the yaw moment of wind turbine rotors, as these are generally capable of modelling the underlying physics of this phenomenon. In addition, the comparative investigation of not only the mean value but also the temporal evolution of the yaw moment may provide deeper insight in the quality of these modelling approaches. Another way to improve the prediction of the yaw moment is the development of corrections for BEMT methods. Even though the Pitt and Peters as well as similar models do not seem to be appropriate, other approaches may solve this issue. In this context, not only the correction itself, but also the determination of the wake skew angle may play an important role. Therefore, further validation of present and the development of new corrections for BEMT methods may be beneficial.

The experimental setup is described in detail in this study and all further relevant information needed for numerical simulations is given in the appendix. Therefore, this work offers a set of validation data on the yaw moment of a downwind coned wind turbine rotor, which is open for all interested researchers and may serve as a basis for future validations.

To finalise the validation of newly developed methods and corrections for the prediction of the yaw moment, additional full scale validations are necessary. A number of superimposing influences have been excluded from the present analysis to be able to observe the basic physical effects causing the yaw moment under controlled conditions. However, the results of a simulation method need to hold in reality, where such influences are present.

ACKNOWLEDGEMENTS

The authors kindly thank the Federal Ministry for Economic Affairs and Energy of Germany (BMWi) for funding the HyStOH project (03SX409A-F) and our partners Cruse Offshore GmbH, aerodyn engineering GmbH, JÖRSS-BLUNCK-ORDEMANN GmbH, DNV- GL and the Institute for Ship Structural Design and Analysis at the Hamburg University of Technology for the excellent cooperation. Furthermore, the authors thank Cruse Offshore GmbH for supporting the manufacture and design of the model turbine. Open access publication funded by the Deutsche Forschungsgemeinschaft (DFG, German Research Foundation) - Projektnummer 491268466 and the Hamburg University of Technology (TUHH) in the funding programme *Open Access Publishing*. Open Access funding enabled and organized by Projekt DEAL. WOA Institution: TECHNISCHE UNIVERSITAET HAMBURG Consortia Name : Projekt DEAL.

PEER REVIEW

The peer review history for this article is available at https://publons.com/publon/10.1002/we.2779.

DATA AVAILABILITY STATEMENT

The data that support the findings of this study are available from the corresponding author on request.

ORCID

Christian W. Schulz https://orcid.org/0000-0002-1565-6710
Moustafa Abdel-Maksoud https://orcid.org/0000-0002-2323-1018

REFERENCES

1. Moriarty PJ, Hansen AC. Aerodyn theroy manual. NREL/TP-500-36881, Golden, USA, National Renewable Energy Laboratory; 2001.
2. Pitt DM, Peters DA. Rotor dynamic inflow derivations and time constants from various inflow models. In: Ninth European Rotorcraft Forum; 1983: 55-1-55-22. Stresa, Italy.
3. Haans W. Wind turbine aerodynamics in yaw. *Ph.D. Thesis*: Technische Universiteit Delft; 2011.
4. Haans W, Sant T, Van Kuik G, Van Bussel G. Measurement of tip vortex paths in the wake of a hawt under yawed flow conditions. *Trans ASME*. 2005; 127:499-521.
5. Schepers JG. Engineering models in wind energy aerodynamics. *Ph.D. Thesis*: Technische Universiteit Delft; 2012.
6. Schepers JG. An engineering model for yawed conditions, developed on basis of wind tunnel measurements. In: 37th Aerospace Sciences Meeting and Exhibit; 1999; Reno, USA.
7. Leishman JG. Challenges in modelling the unsteady aerodynamics of wind turbines. *Wind Energy*. 2002;5:85-132.
8. Netzband S, Schulz CW, Göttsche U, Ferreira González D, Abdel-Maksoud M. A panel method for floating offshore wind turbine simulations with fully integrated aero- and hydrodynamic modelling in time domain. *Ship Technol Res*. 2018;65:123-136.
9. Micallef D, Sant T. A review of wind turbine yaw aerodynamics. In: Aissaoui AG, Tahour A, eds. *Wind turbines - design, control and applications*: IntechOpen; 2016:27-53.
10. Burton T, Jenkins N, Sharpe D, Bossanyi E. *Wind energy handbook*. 2nd ed.: Wiley; 2011.
11. Coleman R, Feingold A, Stempin CW. Evaluation of the induced velocity fields of an idealized helicopter rotor. Tech. Rep. NACA ARRL5E10, USA, National Advisory Committee for Aeronautics; 1945.
12. White F, Blake B. Improved method of predicting helicopter control response and gust sensitivity. In: Proceedings of the 35th Annual Forum of the American Helicopter Soc.; 1979:79-25-1-79-25-12. Washington, DC, USA.
13. Schepers JG. Iea annex xx: Comparison between calculations and measurements on a wind turbine in yaw in the nasa-ames windtunnel. Tech. Rep. ECN-E–07-072, Peten, Netherlands, Energy Reseach Centre of the Netherlands; 2007.

14. Hand MM, Simms DA, Fingersh LJ, et al. Unsteady aerodynamics experiment phase vi: Wind tunnel test configurations and available data campaigns. Tech. Rep. NREL/TP-500-29955, Golden, USA, National Renewable Energy Laboratory; 2001.
15. Ning A, Hayman G, Damiani R, Jonkman J. Development and validation of a new blade element momentum skewed-wake model within aerodyn. In: 33rd ASME Wind Energy Symposium; 2015; Kissimmee, USA.
16. Oye S. Induced velocities for rotors in yaw. In: Procedings of the Sixth IEA Symposium on the Aerodynamics of Wind Turbines; 1992; Petten, Netherlands.
17. Damiani R, Hayman G. The unsteady aerodynamics module for fast 8. NREL/TP-5000-66347, Golden, USA, National Renewable Energy Laboratory; 2019.
18. Tsalicoglou C, Jafari S, Chokani N, Abhari RS. Rans computations of mexico rotor in uniform and yawed inflow. *J Eng Gas Turbines Power*. 2014;136:11202.
19. Ahmed I, Teich M, Lawerenz M. 3d rans simulation of nrel phase-vi and Mexico wind turbines. In: 17th International Symposium on Transport Phenomena and Dynamics of Rotating Machinery (ISROMAC2017); 2012; Maui, USA.
20. Pierella F, Krogstad PA, Saetran L. Blind test 2 calculations for two in-line model wind turbines where the downstream turbine operates at various rotational speeds. *Renew Energy*. 2014;70:62-77.
21. Krogstad PA, Eriksen PE. 'blind test' calculations of the performance and wake development for a model wind turbine. *Renew Energy*. 2013;50:325-333.
22. Zhang Y, Zuijlen A, Bussel G. The mexico rotor aerodynamic loads prediction: Zigzag tape effects and laminar-turbulent transition modeling in cfd. *J Wind Eng Ind Aerod*. 2017;168:152-163.
23. Langtry RB, Menter FR. Correlation-based transition modeling for unstructured parallelized computational fluid dynamics codes. *AIAA J*. 2009;47(12):2897-2096.
24. Schepers JG, Schreck SJ. Aerodynamic measurements on wind turbines. *Wiley Interdiscip Rev Energy Environ*. 2018;8:e320.
25. ELSAMPROJECT A/S. The tjæreborg wind turbine - final report. Tech. Rep. EP92/33, Fredericia, Denmark; 1992.
26. Troldborg N, Bak C, Madsen HA, Skrzypinski W. Danaero mw II: Final report. ISBN 978-87-92896-39-1, Roskilde, Denmark, TU Wind Energy; 2013.
27. Grant I, Parkin P, Wang X. Optical vortex tracking studies of a horizontal axis wind turbine in yaw using laser-sheet, flow visualisation. *Exp Fluids*. 1997;23:513-519.
28. Bastankhah M, Portè-Agel F. Experimental and theoretical study of wind turbine wakes in yawed conditions. *J Fluid Mech*. 2016;806:506-541.
29. Micallef D, Ferreira CS, Sant T, Van Bussel G. Experimental and numerical investigation of tip vortex generation and evolution on horizontal axis wind turbines. *Wind Energy*. 2016;19:1485-1501.
30. Krogstad PA, Lund JA. An experimental and numerical study of the performance of a model turbine. *Wind Energy*. 2012;15:443-457.
31. Krogstad PA, Adaramola MS. Performance and near wake measurements of a model horizontal axis wind turbine. *Wind Energy*. 2012;15:743-756.
32. Bracchi T, Krogstad PA. Yaw moments of a three-axis wind turbine with yaw error. In: Proceedings of the Twenty-second (2012) International Offshore and Polar Engineering Conference; 2012; Rhodes, Greece.
33. Bartl J, Mühle F, Sætran L. Wind tunnel study on power output and yaw moments for two yaw-controlled model wind turbines. *Wind Eng Science*. 2018;3:489-502.
34. Maeda T, Kamada Y, Suzuki J, Fujioka H. Rotor blade sectional performance under yawed inflow conditions. *J Sol Energy Eng*. 2008;130:1-7.
35. Snel H, Schepers JG. Joint investigation of dynamic inflow effects and implementation of an engeneering method. Tech. Rep. ECN-C–94-107, Petten, Netherlands, Energy Reseach Centre of the Netherlands; 1995.
36. Verelst D, Larsen TJ, Van Wingerden JW. Wind tunnel tests of a free yawing downwind wind turbine. *J Phys: Conf Ser*. 2014;555:12103.
37. Verelst D, Larsen TJ, Van Wingerden JW. Open access wind tunnel measurements of a downwind free yawing wind turbine. *J Phys: Conf Ser*. 2016;753:72013.
38. Verelst D. Numerical and experimental results of a passive free yawing downwind wind turbine. *Ph.D. Thesis*: DTUWind Energy; 2013.
39. Kress C, Chokani N, Abhari RS. Downwind wind turbine yaw stability and performance. *Renew Energy*. 2015;83:1157-1165.
40. Schepers JG, Snel H. Model experiments in controlled conditions - final report. Tech. Rep. ECN-E–07-042, Petten, Netherlands, Energy Reseach Centre of the Netherlands; 2008.
41. Lindenburg C. Investigation into rotor blade aerodynamics - analysis of the stationary measurements on the uae phase-vi rotor in the nasa-ames wind tunnel. Tech. Rep. ECN-C–03-025, Peten, Netherlands, Energy Reseach Centre of the Netherlands; 2003.
42. Sørensen NN, Michelsen JA, Schreck S. Navier-stokes predictions of the nrel phase vi rotor in the nasa ames 80 ft x 120 ft wind tunnel. *Wind Energy*. 2002;169:151-169.
43. Gòmez-Iradi S, Steijl R, Barakos GN. Development and validation of a cfd technique for the aerodynamic analysis of hawt. *J Sol Energy Eng*. 2009;131:31009.
44. Lyon CA, Broeren AP, Giguère P, Gopalarathnam A, Selig MS. *Summary of low-speed airfoil data, volume 3*. Virginia Beach, USA: SoarTech Publications; 1997.
45. Drela M. Xfoil: An analysis and design system for low reynolds number airfoils. *Low Reynolds Number Aerodynamics*. Notre Dame, IN, USA; 1989:22016.
46. Rahimi H, Hartvelt M, Peinke J, Schepers JG. Investigation of the current yaw engineering models for simulation of wind turbines in bem and comparison with cfd and experiment. *J Phys Conf Ser*. 2016;753:22016.

How to cite this article: Schulz CW, Wang K, Wieczorek K, Netzband S, Abdel-Maksoud M. Experimental and numerical investigation of the yaw moment of a downwind coned wind turbine rotor. *Wind Energy*. 2022;25(12):1995-2015. doi:10.1002/we.2779

APPENDIX A

TABLE A1 Blade definition for 0° cone angle

Radius [m]	Chord length [m]	Twist angle [°]	Twist centre [%]
0.046	0.050	-	50
0.066	0.050	-	50
0.090	0.130	19.94	27
0.115	0.126	17.02	27
0.140	0.116	14.10	27
0.165	0.101	12.11	27
0.190	0.089	10.13	27
0.215	0.080	8.88	27
0.240	0.072	7.63	27
0.265	0.066	6.99	27
0.290	0.061	6.35	27
0.340	0.052	5.48	27
0.390	0.046	5.02	27
0.440	0.042	4.46	27
0.465	0.040	4.00	27

TABLE A2 Measurement results for selected yaw angles

Yaw angle [°]	Torque [Nm]	Thrust [N]	Yaw moment [Nm]	Lateral force [N]	Rotational Speed [RPM]	Wind speed [m s^{-1}]
−55	0.2018	11.22	−0.2014	−1.934	1204.87	9.271
−50	0.3199	13.61	−0.2475	−1.816	1207.33	9.274
−45	0.4382	15.69	−0.2787	−1.700	1203.67	9.277
−40	0.5552	17.68	−0.2942	−1.565	1202.13	9.308
−35	0.6578	19.48	−0.2905	−1.449	1205.78	9.293
−30	0.7518	20.89	−0.2683	−1.301	1204.09	9.277
−25	0.8291	22.13	−0.2394	−1.160	1205.97	9.302
−20	0.9017	23.18	−0.2048	−0.975	1201.21	9.301
−15	0.9556	23.98	−0.1611	−0.798	1201.58	9.342
−10	0.9919	24.47	−0.1074	−0.632	1196.98	9.301
−5	1.0080	24.87	−0.0564	−0.442	1203.92	9.285
−3	1.0120	24.91	−0.0339	−0.386	1201.40	9.288
0	1.0195	24.95	0.0046	−0.309	1198.30	9.274
3	1.0151	24.96	0.0427	−0.173	1202.56	9.297
5	1.0104	24.94	0.0648	−0.074	1203.75	9.319
8	1.0019	24.69	0.0972	0.061	1199.77	9.297
10	0.9884	24.50	0.1185	0.137	1203.19	9.335
15	0.9461	23.95	0.1686	0.323	1201.29	9.298
20	0.8950	23.22	0.2157	0.495	1204.07	9.298
25	0.8273	22.25	0.2539	0.802	1202.28	9.312
30	0.7465	20.97	0.2818	0.813	1201.22	9.290
35	0.6486	19.53	0.3024	0.982	1202.56	9.319
40	0.5402	17.84	0.3100	1.169	1209.34	9.297
45	0.4279	15.83	0.2879	1.317	1203.72	9.290
50	0.3104	13.82	0.2554	1.411	1208.27	9.316
55	0.1931	11.54	0.2161	1.534	1204.72	9.288